Supporting Information:

Copper-Hydroperoxo Mediated *N*-Debenzylation Chemistry Mimicking Aspects of Copper Monoxygenases

Debabrata Maiti, Amy A. Narducci Sarjeant and Kenneth D. Karlin *

Department of Chemistry, The Johns Hopkins University, Baltimore, MD 21218.

*Corresponding Author: karlin@jhu.edu

X-ray Crystal Structure of $[(L^{NH(CH2Ph)})Cu^{II}(Cl)]ClO_4$ (10). The chloride (Cl1), alkylamino nitrogen (N2) and pyridyl groups not substituted in the 6-position (N1 and N3) comprise the basal plane in the five-coordinate complex. Five-coordinated copper(II) ion has a slightly distorted square pyramidal geometry (τ = 0.197), with weak axial Cu^{II}-Npy' interaction (Cu-N4 = 2.412(2)). Selected bond distances and angles are listed in Table S1.

Table S1. Selected Distances and Angles for $[(L^{NH(CH_2Ph)})Cu^{II}(Cl)]^+$ (**10**).

Bond Lengths (Å)		**Bond Angles (deg)**	
Cu(1)-N(1)	1.9880(18)	N(1)-Cu(1)-N(3)	163.34(8)
Cu(1)-N(3)	1.9993(18)	N(1)-Cu(1)-N(2)	82.05(7)
Cu(1)-N(2)	2.0503(18)	N(3)-Cu(1)-N(2)	83.47(7)
Cu(1)-Cl(1)	2.2311(8)	N(1)-Cu(1)-Cl(1)	96.36(6)
Cu(1)-N(4)	2.412(2)	N(3)-Cu(1)-Cl(1)	97.40(6)
N(1)-C(5)	1.349(3)	N(2)-Cu(1)-Cl(1)	175.17(5)

Table S2. Selected Distances and Angles for $[(L^{N(CH_2Ph)_2})Cu^{II}(H_2O)(ClO_4)]^+$ (**1**).

Bond Lengths (Å)		**Bond Angles (deg)**	
Cu(1)-O(1)	1.9723(11)	O(1)-Cu(1)-N(1)	94.34(5)
Cu(1)-N(1)	1.9885(12)	O(1)-Cu(1)-N(3)	99.06(5)
Cu(1)-N(3)	1.9965(12)	N(1)-Cu(1)-N(3)	166.31(5)
Cu(1)-N(2)	2.0104(12)	O(1)-Cu(1)-N(2)	175.69(5)
Cu(1)-O(2)	2.3515(11)	N(1)-Cu(1)-N(2)	83.57(5)
O(1)-H(1B)	0.78(2)	N(3)-Cu(1)-N(2)	83.24(5)
O(1)-H(1O)	0.77(3)	O(1)-Cu(1)-O(2)	86.88(5)
N(1)-C(5)	1.3429(19)	N(1)-Cu(1)-O(2)	94.29(4)

N(1)-C(1)	1.3459(19)	N(3)-Cu(1)-O(2)	83.72(5)
N(2)-C(7)	1.4844(18)	N(2)-Cu(1)-O(2)	97.03(5)
N(2)-C(6)	1.4929(18)	Cu(1)-O(1)-H(1B)	120.4(16)

Table S3. Selected Distances and Angles for [($\mathbf{L}^{\mathbf{N(CH_3)_2}}$)$Cu^{II}$(HCOO$^-$)($ClO_4$)$Cu^{II}$($\mathbf{L}^{\mathbf{NH(CH_3)}}$)] ($ClO_4$)$_2$.

Bond Lengths (Å)		**Bond Angles (deg)**	
Cu(1)-O(2)	1.942(2)	O(2)-Cu(1)-N(3)	96.00(11)
Cu(1)-N(3)	2.020(3)	O(2)-Cu(1)-N(2)	175.51(13)
Cu(1)-N(2)	2.022(3)	N(3)-Cu(1)-N(2)	82.15(12)
Cu(1)-N(1)	2.023(3)	O(2)-Cu(1)-N(1)	99.39(11)
Cu(1)-N(4)	2.181(3)	N(3)-Cu(1)-N(1)	139.38(12)
Cu(2)-O(1)	1.953(2)	N(2)-Cu(1)-N(1)	84.59(13)
Cu(2)-N(8)	1.980(4)	O(2)-Cu(1)-N(4)	95.93(12)
Cu(2)-N(6)	1.981(4)	N(3)-Cu(1)-N(4)	116.10(12)
Cu(2)-N(7)	2.020(3)	N(2)-Cu(1)-N(4)	81.29(15)
O(1)-C(40)	1.249(5)	N(1)-Cu(1)-N(4)	99.44(11)
O(2)-C(40)	1.261(4)	O(1)-Cu(2)-N(8)	92.25(13)
N(1)-C(1)	1.338(5)	O(1)-Cu(2)-N(6)	101.17(12)
N(1)-C(5)	1.344(4)	N(8)-Cu(2)-N(6)	165.50(14)
N(2)-C(13)	1.471(6)	O(1)-Cu(2)-N(7)	168.96(12)
N(2)-C(7)	1.483(6)	N(8)-Cu(2)-N(7)	83.25(17)
N(2)-C(6)	1.497(5)	N(6)-Cu(2)-N(7)	82.57(16)
N(3)-C(8)	1.343(5)	C(40)-O(1)-Cu(2)	124.3(2)
N(3)-C(12)	1.343(4)	C(40)-O(2)-Cu(1)	126.3(2)

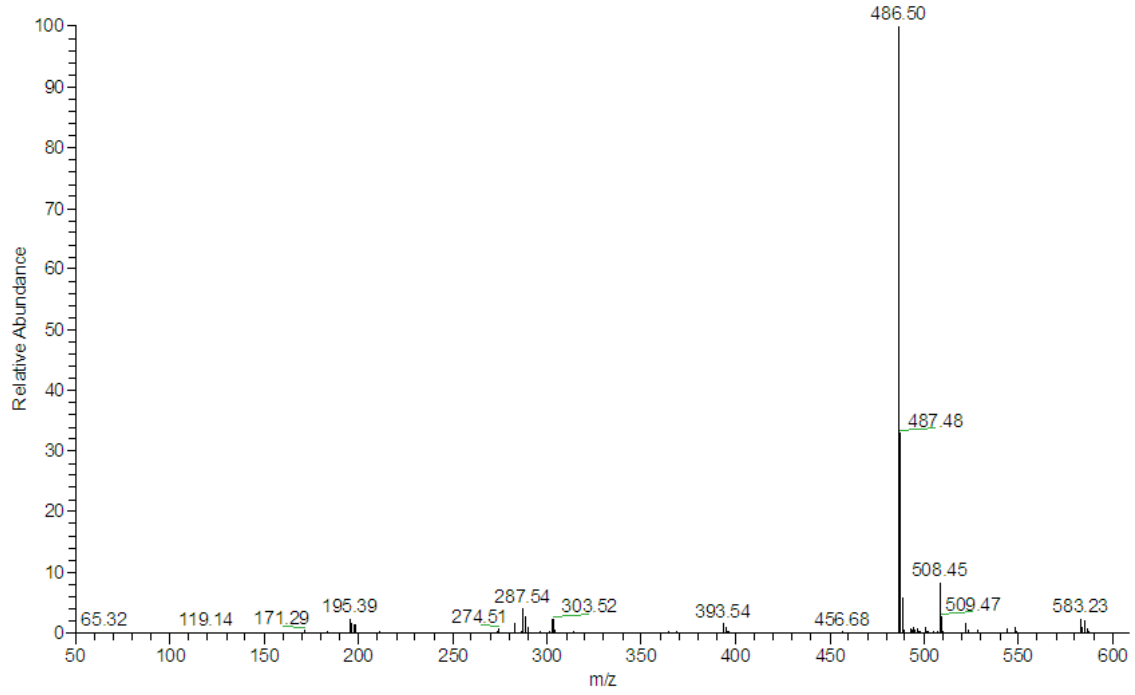

Figure S1. ESI-MS spectrum of $\mathbf{L^{N(CH_2Ph)_2}}$; $[\mathbf{L^{N(CH_2Ph)_2}} + H]^+$ and $[\mathbf{L^{N(CH_2Ph)_2}} + Na]^+$.

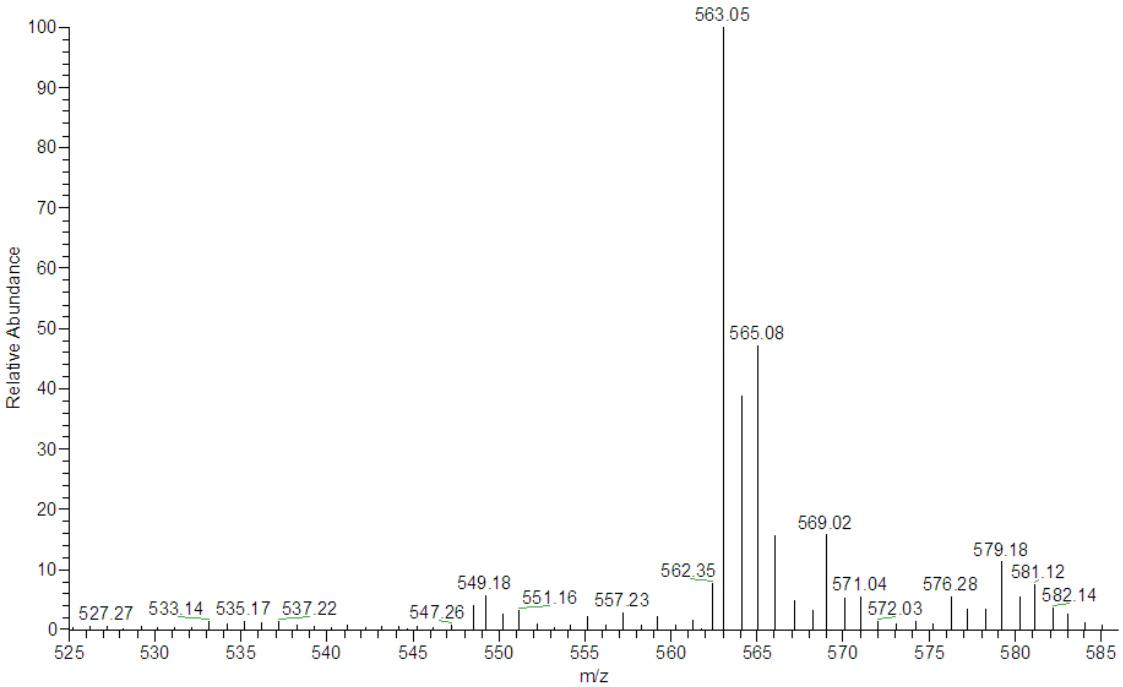

Figure S2. ESI-MS spectrum of $[(\mathbf{L^{N(CH_2Ph)(PhCHO^-)}}Cu^{II}]^+$ (**4**) in acetone obtained from the decomposition of $[(\mathbf{L^{N(CH_2Ph)_2}})Cu^{II}(^-OOH)]^+$ (**2**).

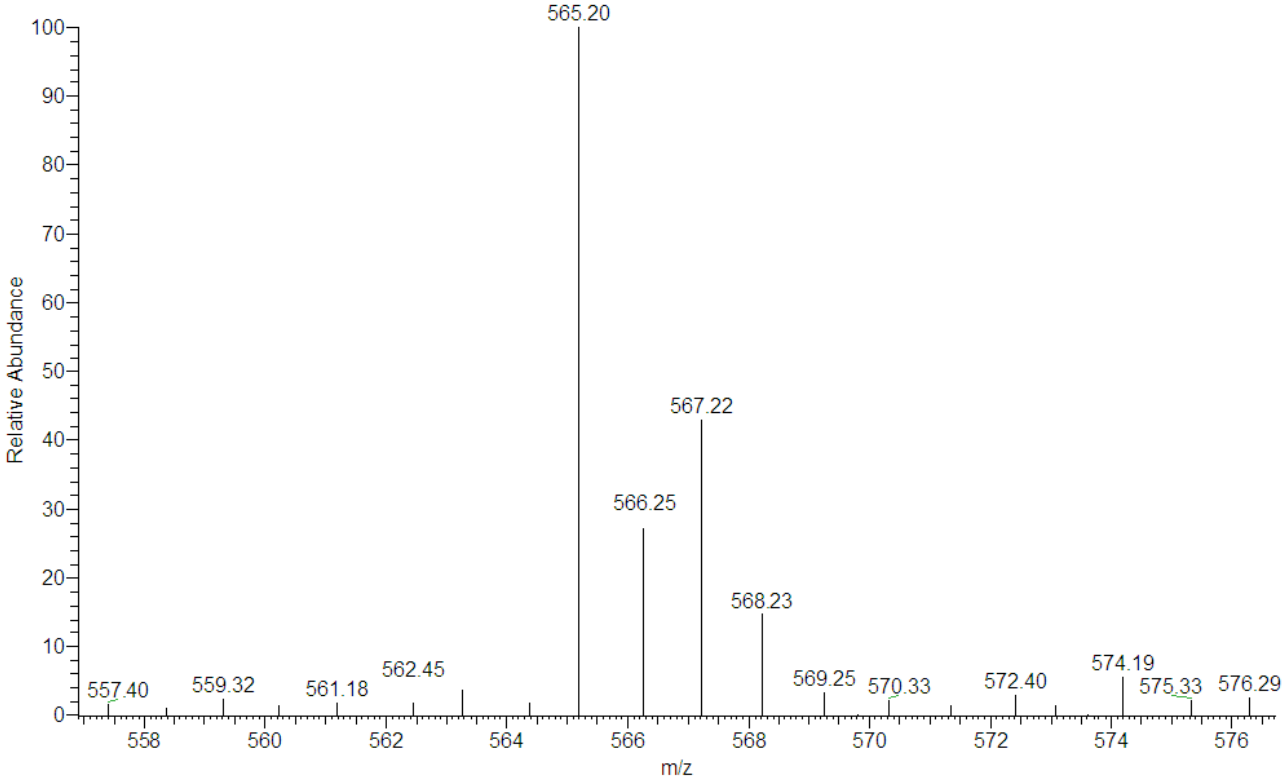

Figure S3. ESI-MS spectrum of $[(\mathbf{L}^{\mathbf{N(CH_2Ph)(PhCH(18)O^-)}}Cu^{II}]^+$ in acetone obtained from the decomposition of $[(\mathbf{L}^{\mathbf{N(CH_2Ph)_2}})Cu^{II}(^{-18}O^{18}OH)]^+$.

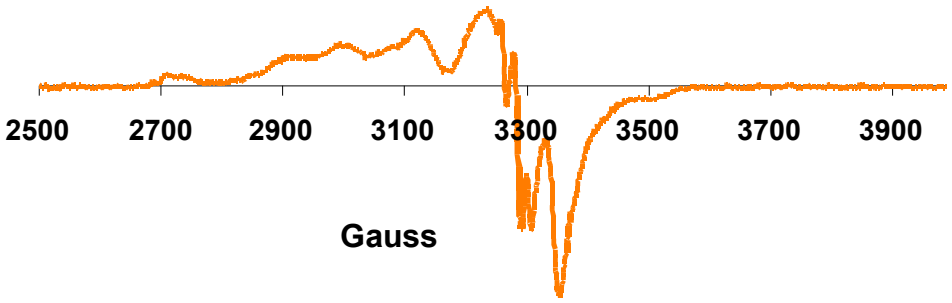

Figure S4. EPR spectrum of the decomposition products from $[(\mathbf{L}^{\mathbf{N(CH_2Ph)_2}})Cu^{II}(^{-}OOH)]^+$ (**2**) in acetone at 77 K.

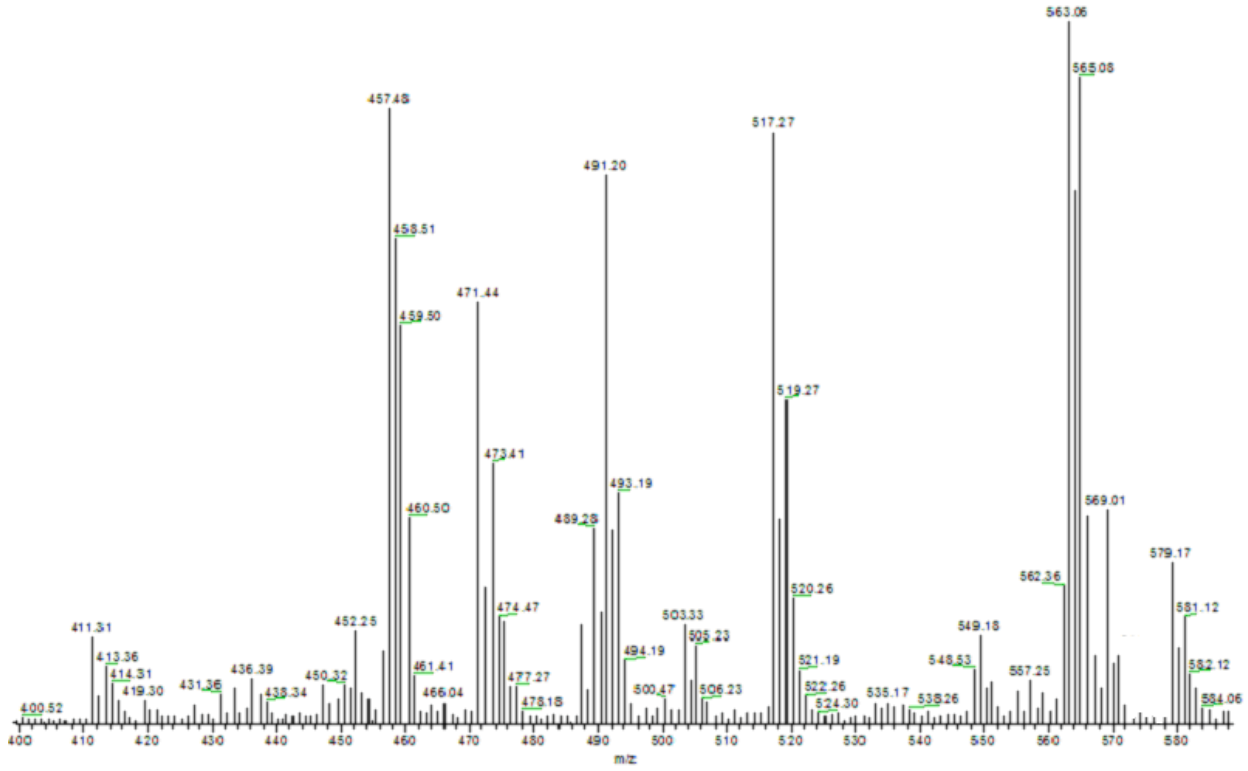

Figure S5. ESI-MS spectrum of the decomposition products from $[(\mathbf{L}^{\mathbf{N(CH_2Ph)_2}})Cu^{II}(^{-}OOH)]^{+}$ (**2**) in acetone.

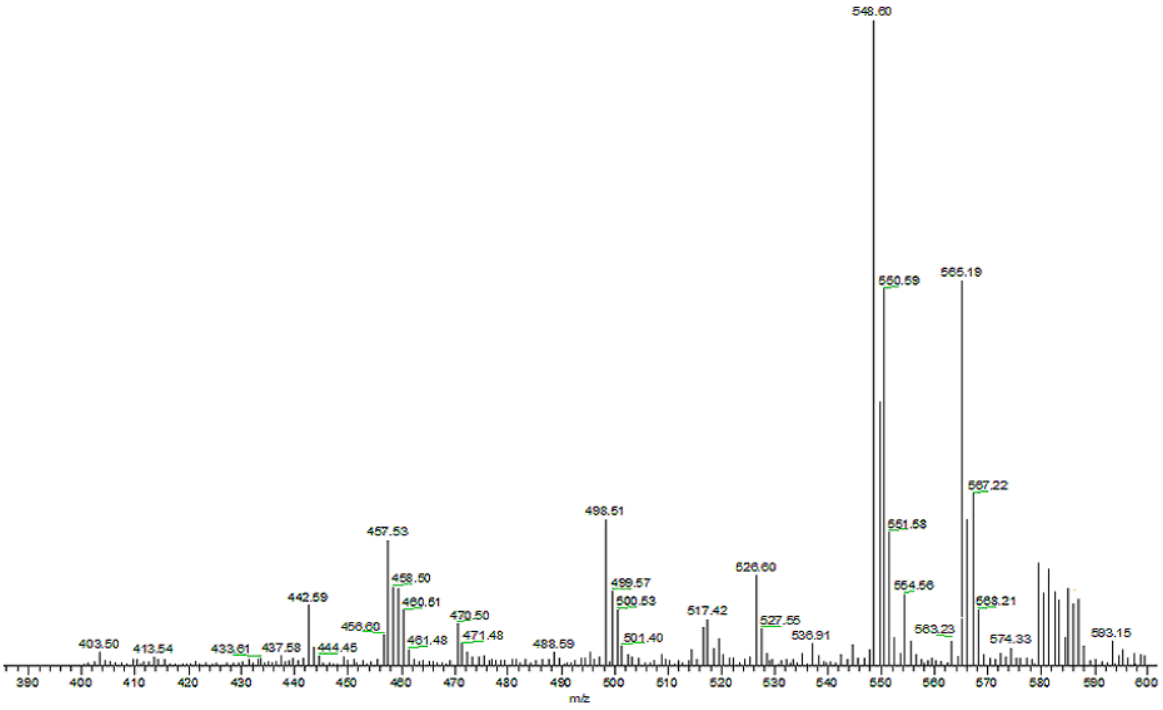

Figure S6. ESI-MS spectrum of the decomposition products from $[(\mathbf{L}^{\mathbf{N(CH_2Ph)_2}})Cu^{II}(^{-}{}^{18}O{}^{18}OH)]^{+}$ (**2**) in acetone.

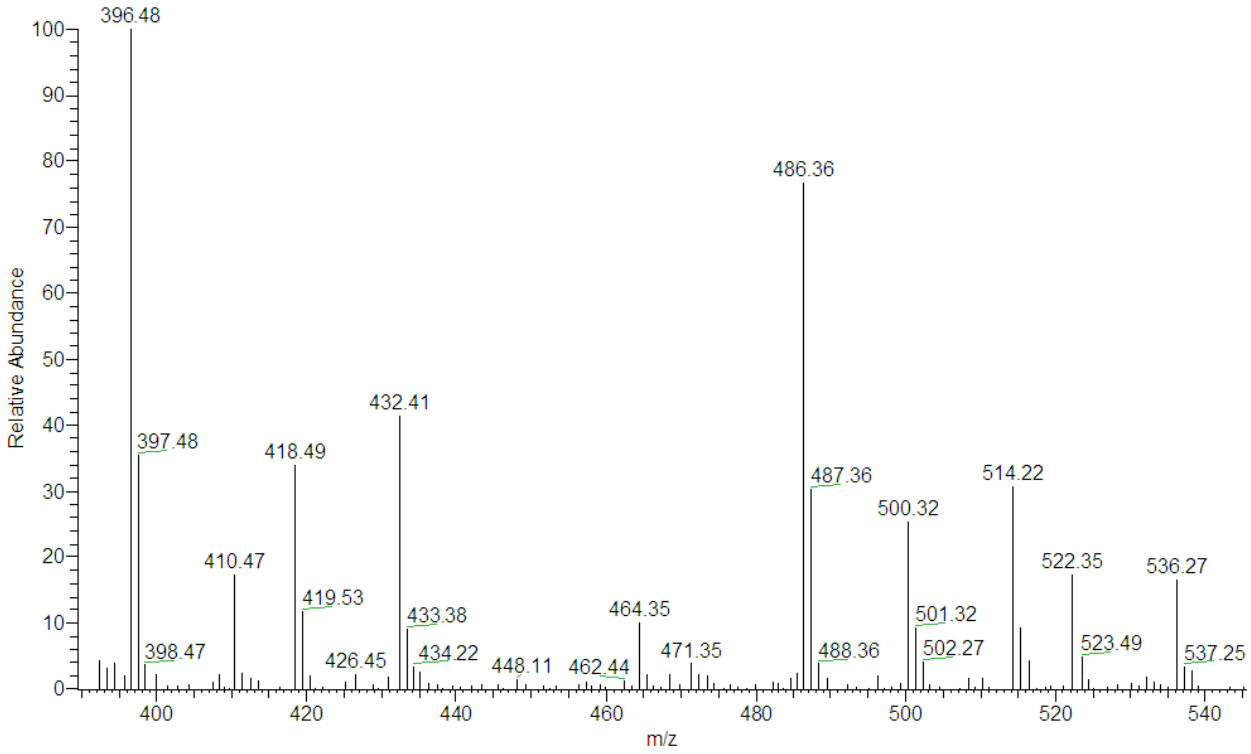

Figure S7. ESI-MS spectrum of the extracted organics from the decomposition of $[(\mathbf{L}^{\mathbf{N(CH_2Ph)_2}})Cu^{II}(^{-}OOH)]^{+}$ (**2**) in acetone.

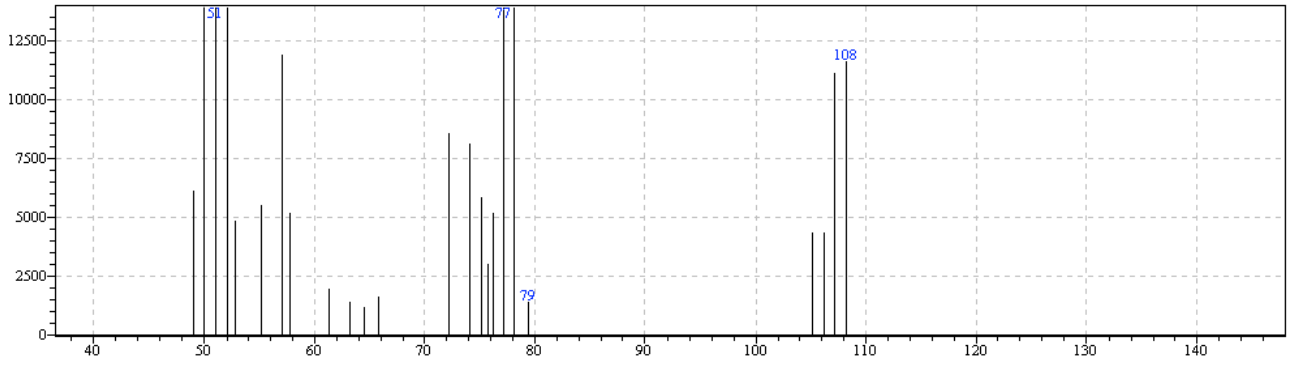

Figure S8. GC-MS spectrum of $PhCH^{18}O$ from the decomposition of $[(\mathbf{L}^{\mathbf{N(CH_2Ph)_2}})Cu^{II}(^{-18}O^{18}OH)]^{+}$.

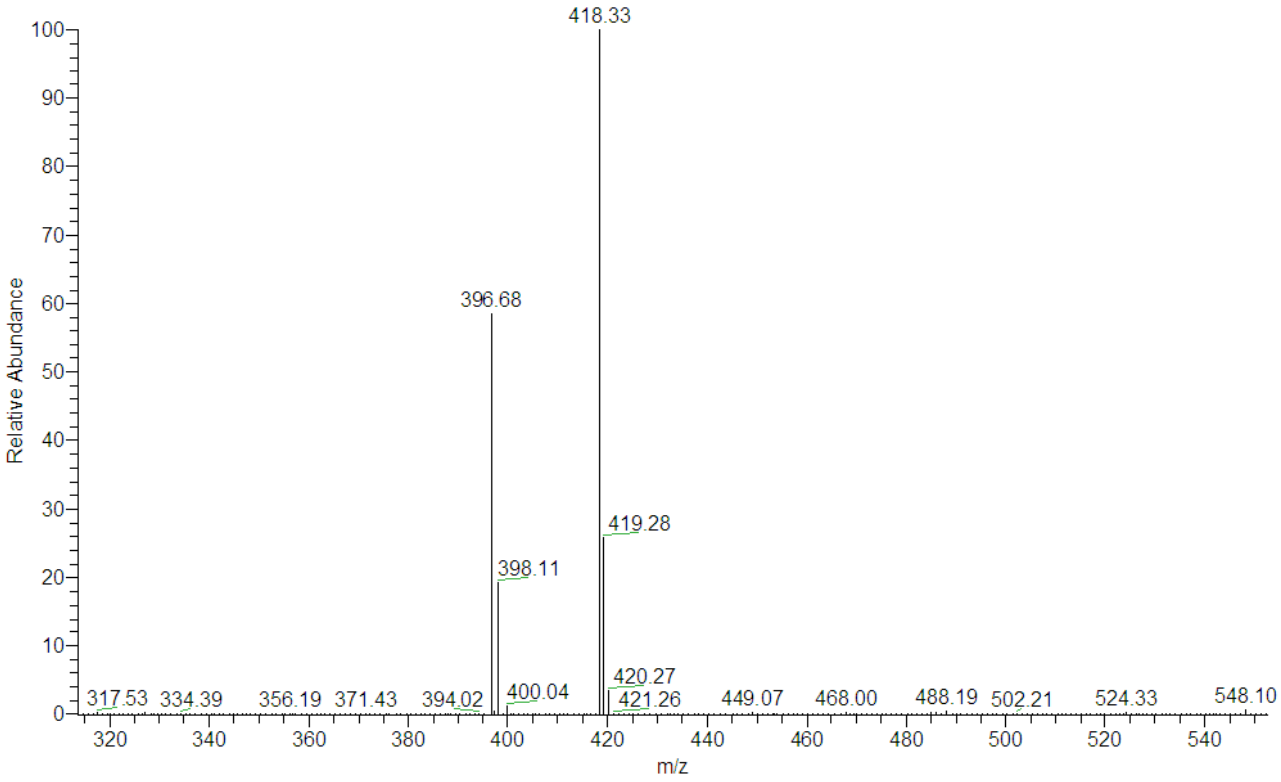

Figure S9. ESI-MS spectrum of $\mathbf{L}^{\mathbf{NH(CH_2Ph)}}$; $[\mathbf{L}^{\mathbf{NH(CH_2Ph)}} + H]^+$ and $[\mathbf{L}^{\mathbf{NH(CH_2Ph)}} + Na]^+$.

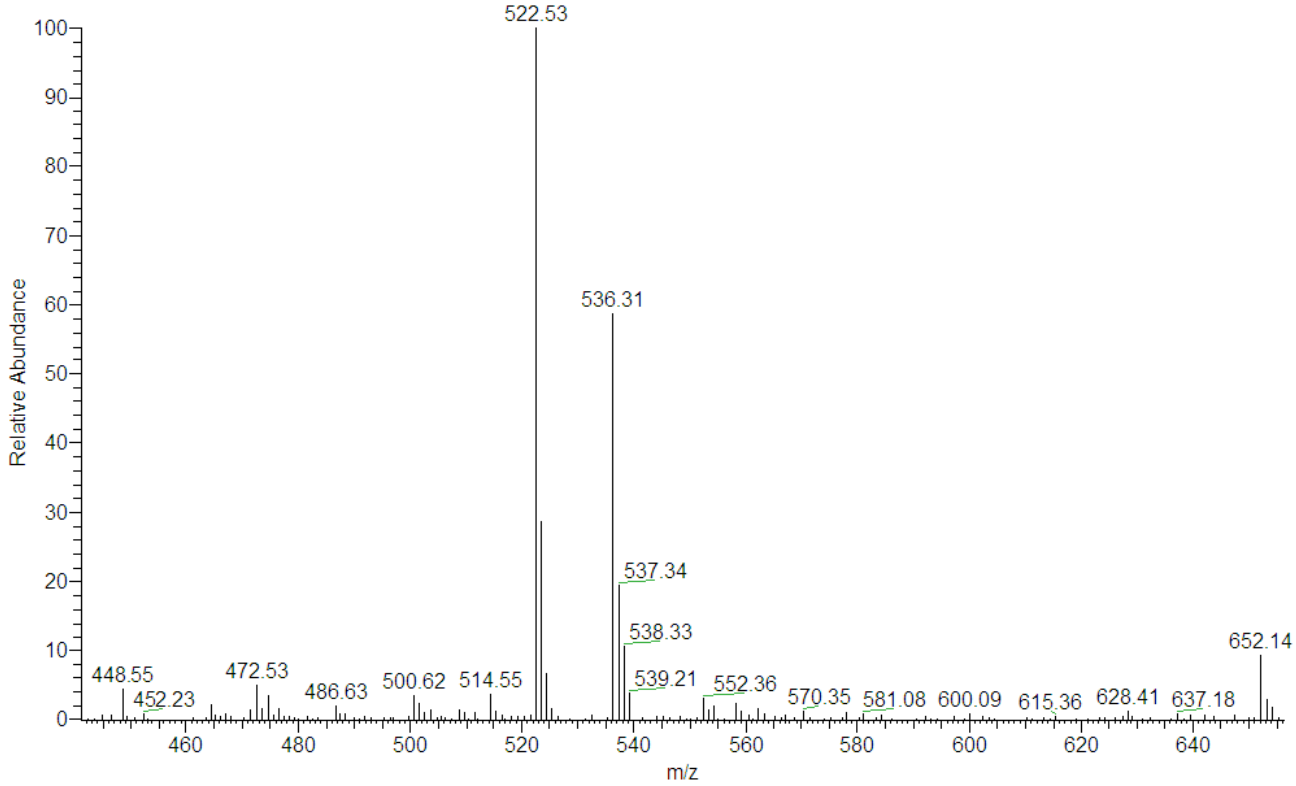

Figure S10. ESI-MS spectrum $\mathbf{L}^{\mathbf{N(CH_2Ph)(COPh)}}$ and $\mathbf{L}^{\mathbf{N(COPh)_2}}$; $[\mathbf{L}^{\mathbf{N(CH_2Ph)(COPh)}} + Na]^+$ and $[\mathbf{L}^{\mathbf{N(COPh)_2}} + Na]^+$.

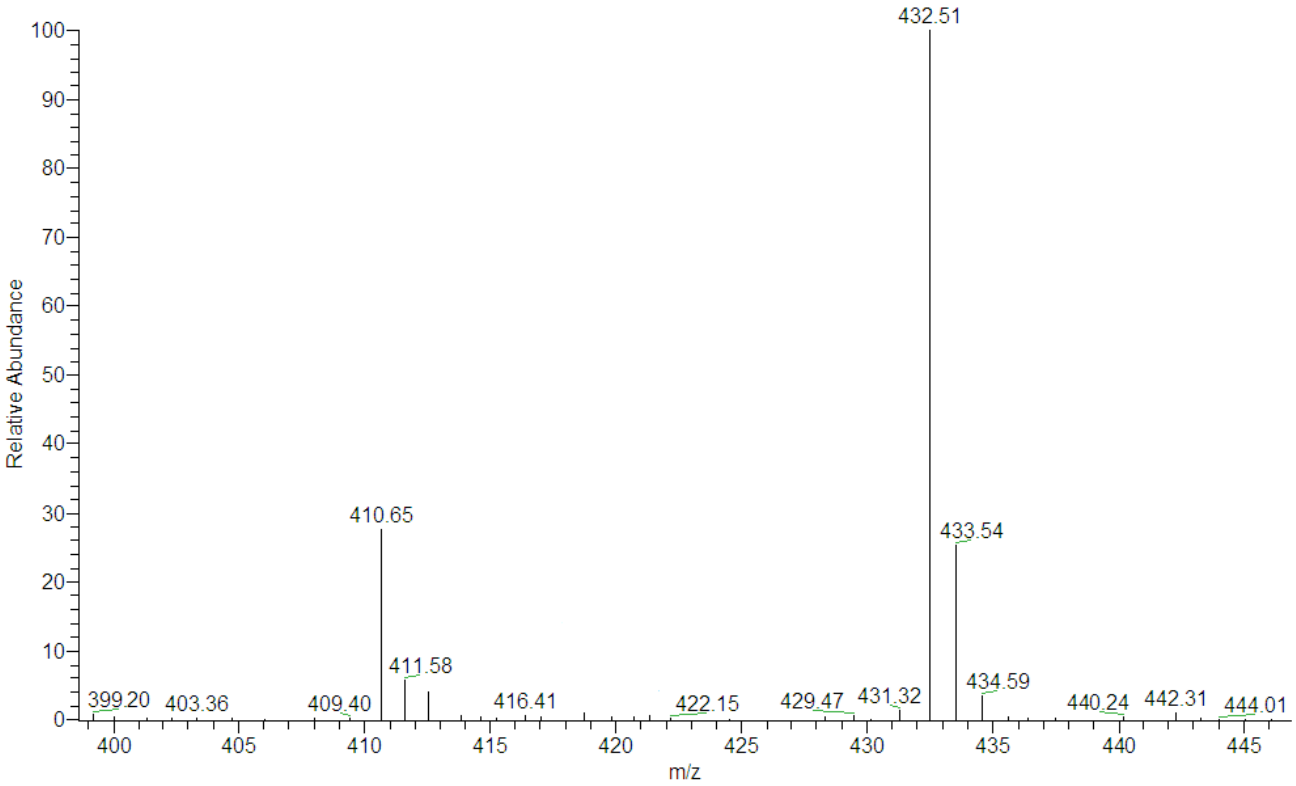

Figure S11. ESI-MS spectrum $\mathbf{L}^{\mathbf{NH(COPh)}}$; $[\mathbf{L}^{\mathbf{NH(COPh)}} + H]^+$ and $[\mathbf{L}^{\mathbf{NH(COPh)}} + Na]^+$.

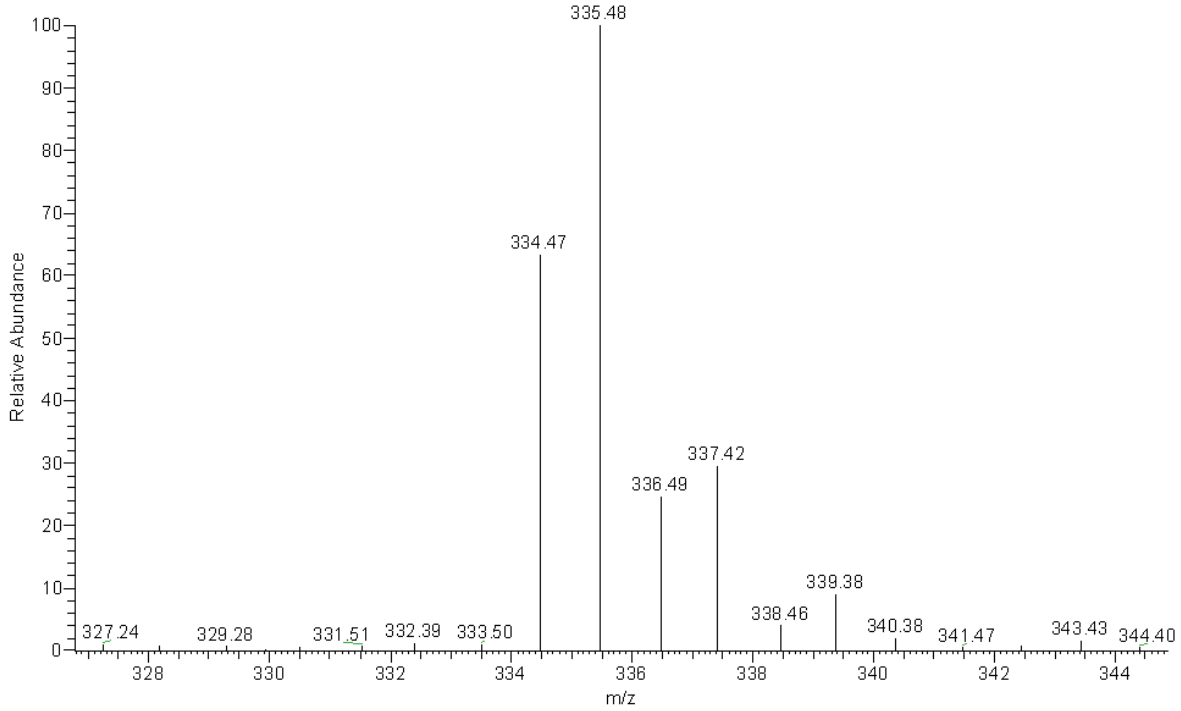

Figure S12. ESI-MS spectrum of Unreacted $\mathbf{L}^{\mathbf{N(CH_3)(CD_3)}}$ showing scrambling of deuterium labeling in $\mathbf{L}^{\mathbf{N(CH_3)(CD_3)}}$ to $\mathbf{L}^{\mathbf{N(CH_3)(CD_2H)}}$ (m/z = 336, M+H), $\mathbf{L}^{\mathbf{N(CH_3)(CDH_2)}}$ (m/z = 335, M+H) and $\mathbf{L}^{\mathbf{N(CH_3)_2}}$ (m/z = 334, M+H).

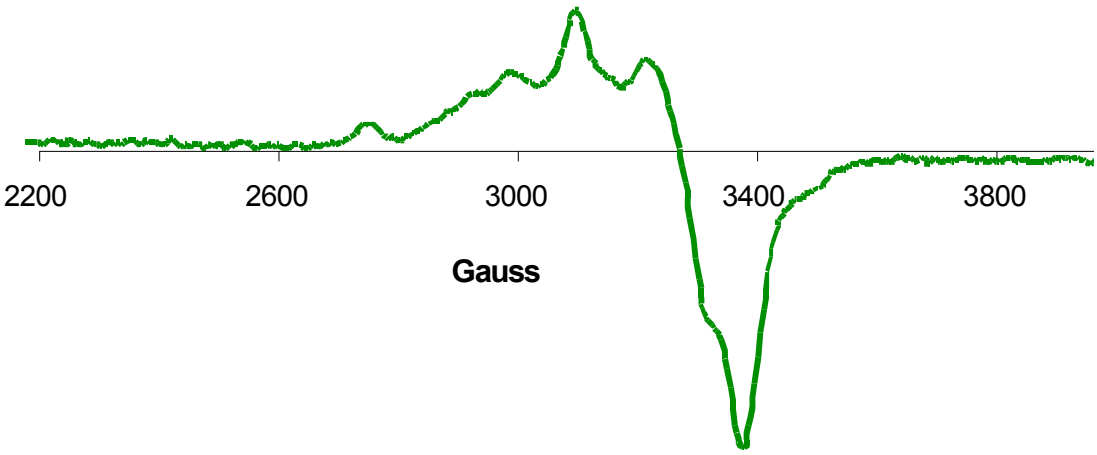

Figure S13. EPR spectrum of $[(\mathbf{L}^{\mathbf{N(CH_3)_2}})Cu^{II}(HCOO^{-})(ClO_4)Cu^{II}(\mathbf{L}^{\mathbf{NH(CH_3)}})]$ $(ClO_4)_2$ in acetone at 77 K.

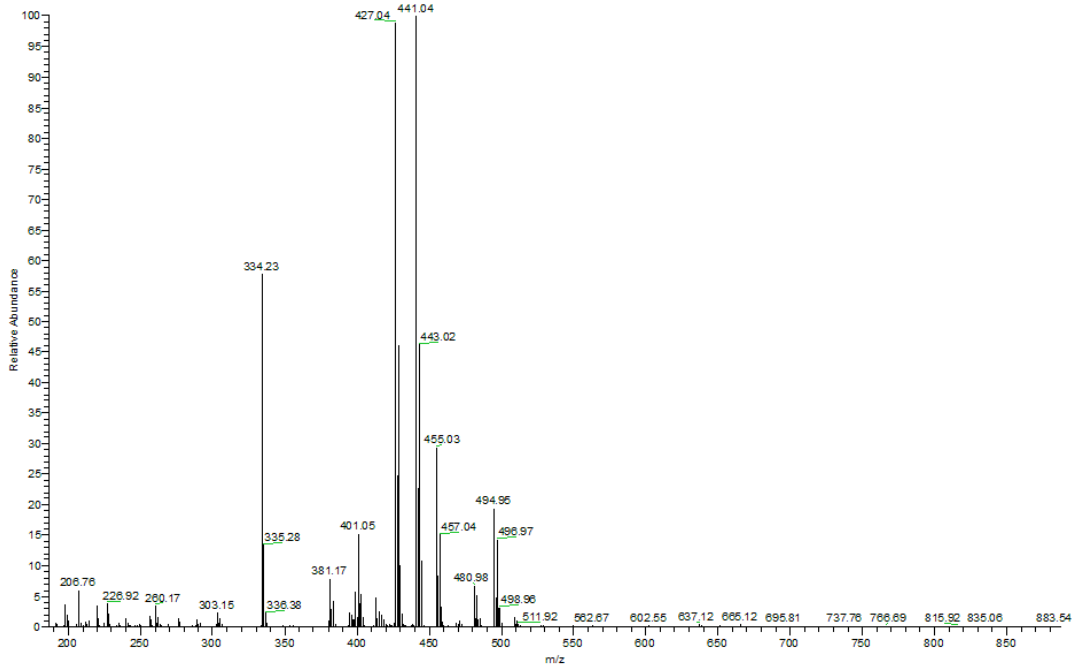

Figure S14. ESI-MS spectrum of the crystalline material from the decomposition of $[(\mathbf{L}^{\mathbf{N(CH_3)_2}})Cu^{II}(^{-}OOH)]^{+}$ (**3**) in acetone.

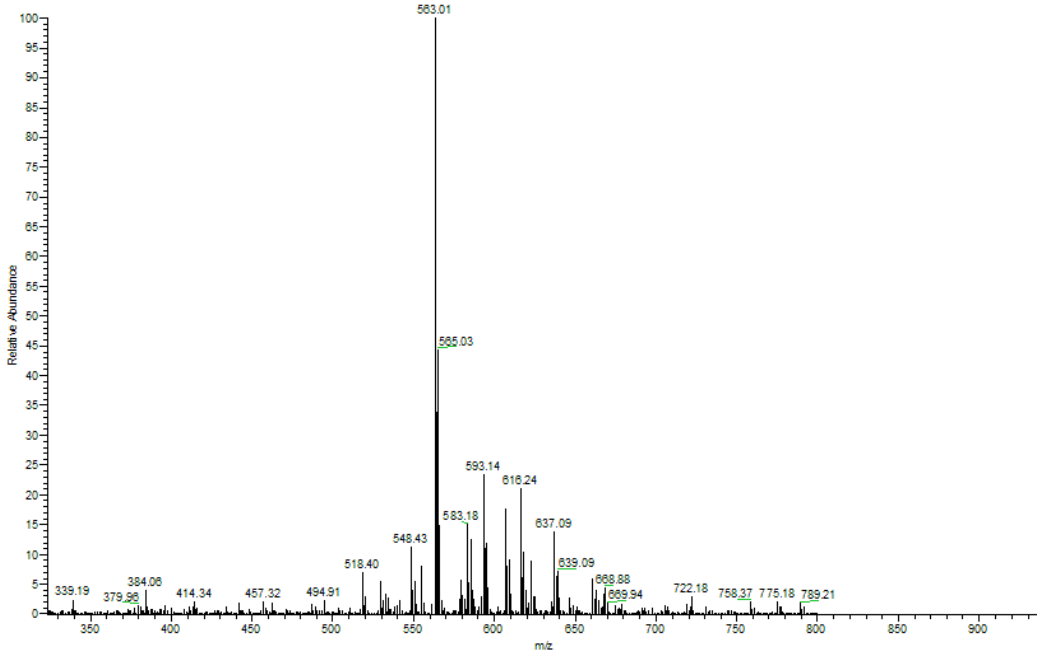

Figure S15. ESI-MS spectrum (with dominant peak at m/z = 563.01) of $[(\mathbf{L}^{\mathbf{N(CH_2Ph)(PhCHO^-)}}Cu^{II}]^+$ (**4**) in acetonitrile obtained from the PhIO reaction with $[(\mathbf{L}^{\mathbf{N(CH_2Ph)_2}})Cu^{I}]^+$ (**6**).

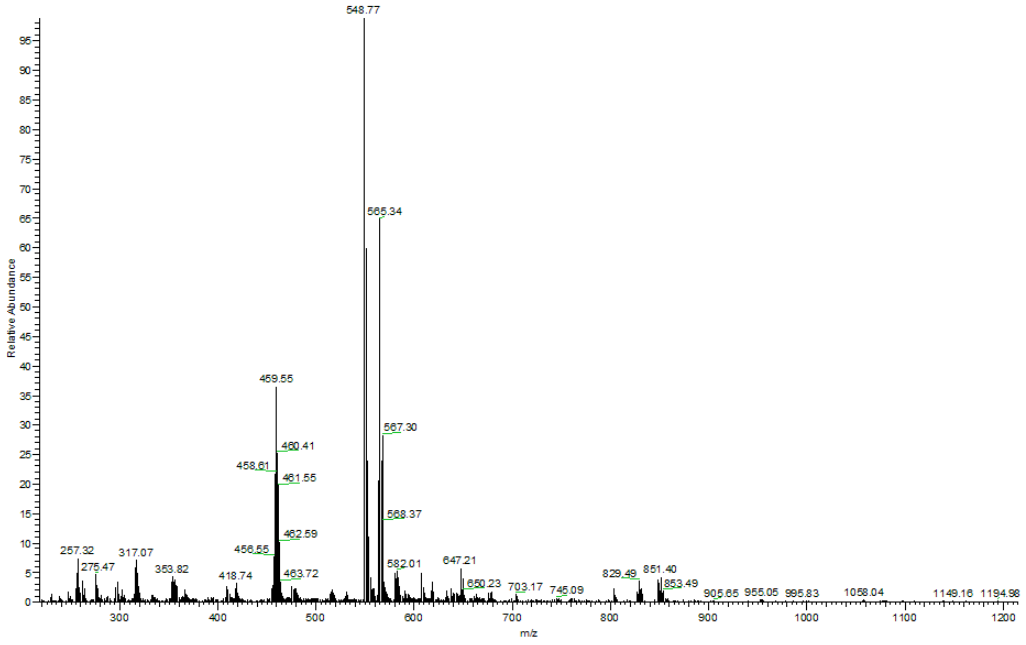

Figure S16. ESI-MS spectrum (with strong peak at m/z = 565.34) of $[(\mathbf{L}^{\mathbf{N(CH_2Ph)(PhCH(18)O^-)}}Cu^{II}]^+$ (**4**) in acetonitrile obtained from the PhIO plus $H_2{}^{18}O$ reaction with $[(\mathbf{L}^{\mathbf{N(CH_2Ph)_2}})Cu^{I}]^+$ (**6**).

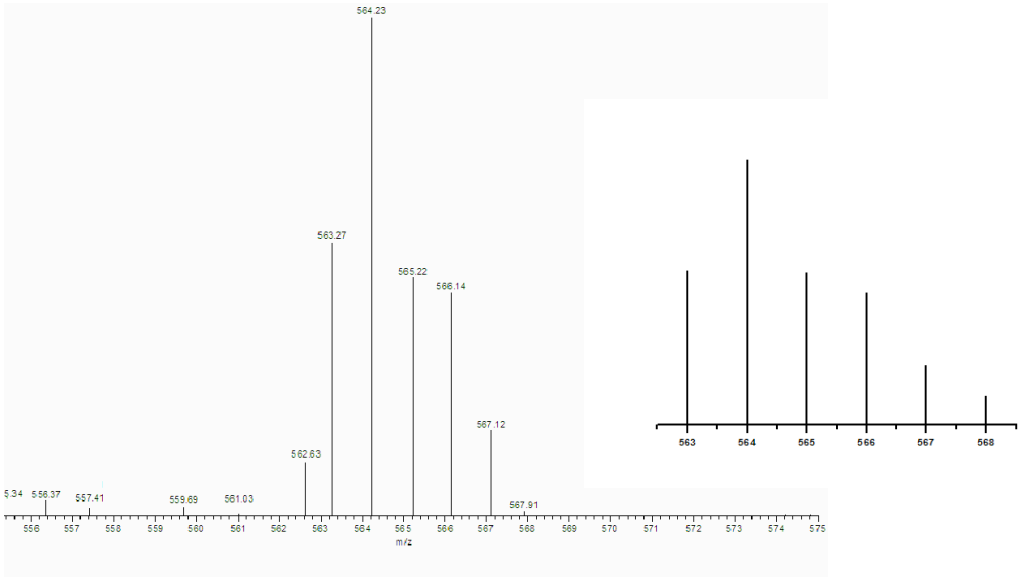

Figure S17. ESI-MS spectra from the reaction of $[(\mathbf{L}^{\mathbf{N(CH_2Ph)_2}})\mathrm{Cu}^{\mathrm{I}}]^+$ (**6**) with PhIO (after ~1.6 min) suggesting the transient formation of the cupryl complex $[(\mathbf{L}^{\mathbf{N(CH_2Ph)_2}})\mathrm{Cu}^{\mathrm{II}}\text{-}\mathrm{O}\bullet]^+$ (**8**) at *m*/*z* = 564.23 (~60% formation) and $[(\mathbf{L}^{\mathbf{N(CH_2Ph)(PhCHO-)}})\mathrm{Cu}^{\mathrm{II}}]^+$ (**4**) at *m*/*z* = 563.27 (~40% formation). Insets showing the expected pattern for 60% formation of **8** plus 40% formation of **4**. See text for further discussion.

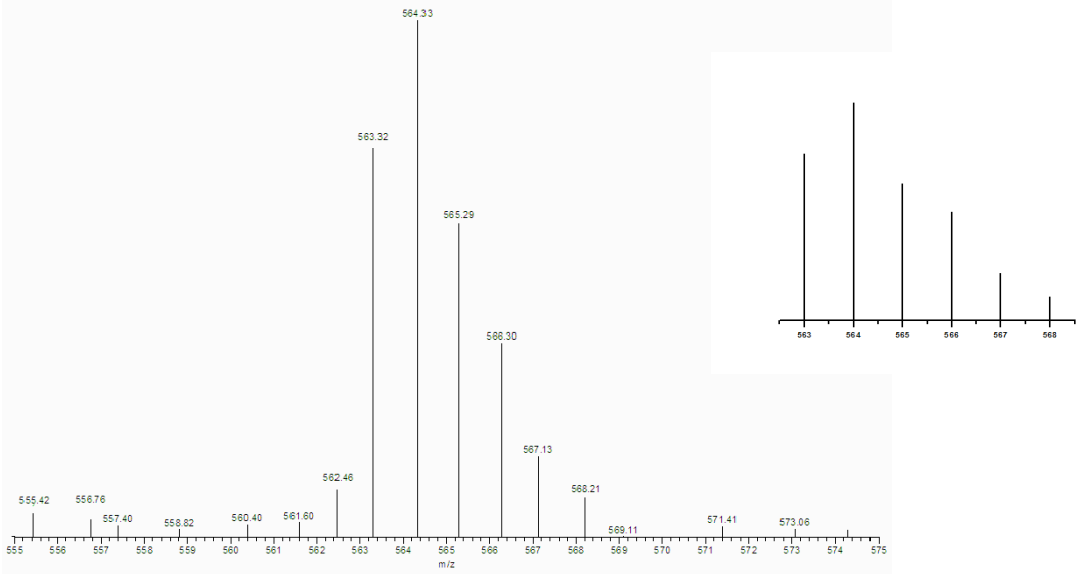

Figure S18. ESI-MS spectra from the reaction of $[(\mathbf{L}^{\mathbf{N(CH_2Ph)_2}})\mathrm{Cu}^{\mathrm{I}}]^+$ (**6**) with PhIO (after ~1.8 min) suggesting the transient formation of the cupryl complex $[(\mathbf{L}^{\mathbf{N(CH_2Ph)_2}})\mathrm{Cu}^{\mathrm{II}}\text{-}\mathrm{O}\bullet]^+$ (**8**) at *m*/*z* = 564.33 (~50% formation) and $[(\mathbf{L}^{\mathbf{N(CH_2Ph)(PhCHO-)}})\mathrm{Cu}^{\mathrm{II}}]^+$ (**4**) at *m*/*z* = 563.32 (~50% formation). Insets showing the expected pattern for 50% formation of **8** plus 50% formation of **4**. See text for further discussion.

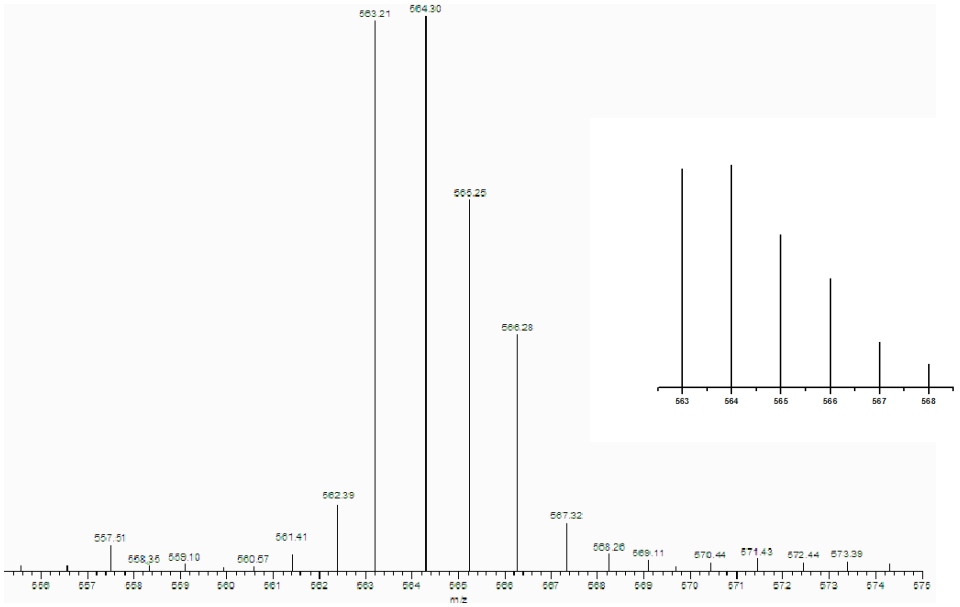

Figure S19. ESI-MS spectra from the reaction of $[(\mathbf{L}^{\mathbf{N(CH_2Ph)_2}})Cu^{I}]^{+}$ (**6**) with PhIO (after ~2.1 min) suggesting the transient formation of the cupryl complex $[(\mathbf{L}^{\mathbf{N(CH_2Ph)_2}})Cu^{II}\text{-}O\bullet]^{+}$ (**8**) at *m/z* = 564.30 (~40% formation) and $[(\mathbf{L}^{\mathbf{N(CH_2Ph)(PhCHO-)}})Cu^{II}]^{+}$ (**4**) at *m/z* = 563.21 (~60% formation). Insets showing the expected pattern for 40% formation of **8** plus 60% formation of **4**. See text for further discussion.

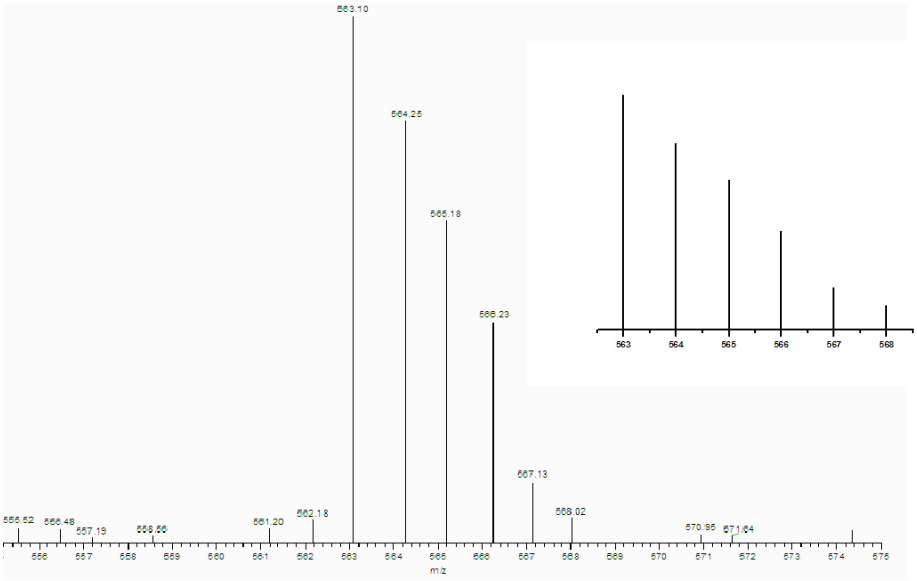

Figure S20. ESI-MS spectra from the reaction of $[(\mathbf{L}^{\mathbf{N(CH_2Ph)_2}})Cu^{I}]^{+}$ (**6**) with PhIO (after ~2.4 min) suggesting the transient formation of the cupryl complex $[(\mathbf{L}^{\mathbf{N(CH_2Ph)_2}})Cu^{II}\text{-}O\bullet]^{+}$ (**8**) at *m/z* = 564.25 (~30% formation) and $[(\mathbf{L}^{\mathbf{N(CH_2Ph)(PhCHO-)}})Cu^{II}]^{+}$ (**4**) at *m/z* = 563.10 (~70% formation). Insets showing the expected pattern for 30% formation of **8** plus 70% formation of **4**. See text for further discussion.

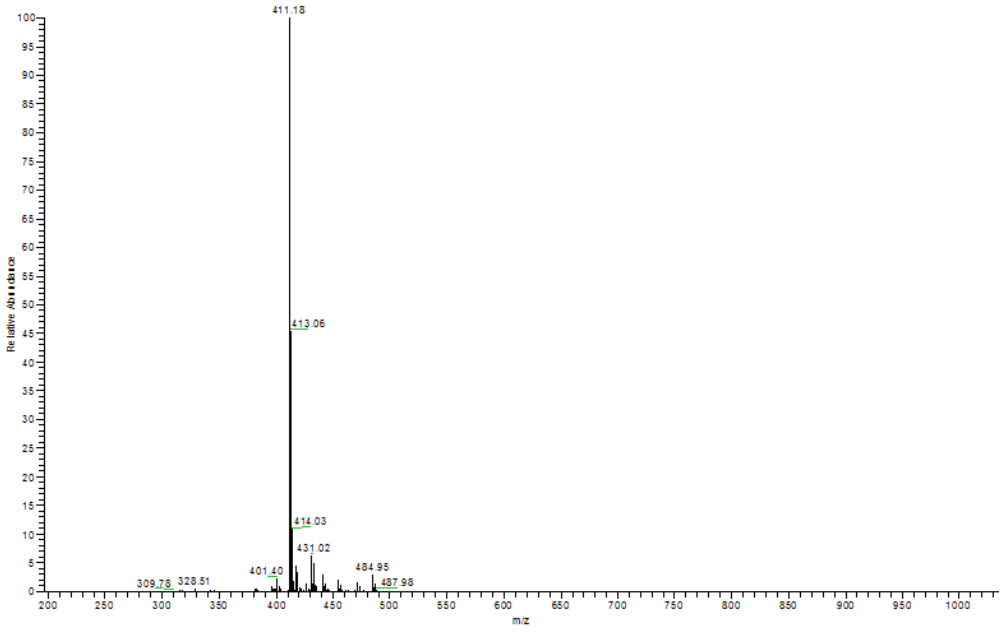

Figure S21. ESI-MS spectrum (with dominant peak at m/z = 411.18) of [($\mathbf{L}^{\mathbf{N(CH_3)(CH_2O^-)}}$)$Cu^{II}$]$^+$ (**5**) in acetonitrile obtained from the PhIO reaction with [($\mathbf{L}^{\mathbf{N(CH_3)_2}}$)$Cu^{I}$]$^+$ (**7**).